# First-principles prediction of the Raman shifts in parahydrogen clusters

Nabil Faruk,[1] Matthew Schmidt,[1] Hui Li,[1,2] Robert J. Le Roy,[1] and Pierre-Nicholas Roy[1,a)]
[1]*Department of Chemistry, University of Waterloo, Waterloo, Ontario N2L 3G1, Canada*
[2]*Institute of Theoretical Chemistry, State Key Laboratory of Theoretical and Computational Chemistry, Jilin University, 2519 Jiefang Road, Changchun 130023, People's Republic of China*

(Received 21 April 2014; accepted 16 June 2014; published online 7 July 2014)

We report a first-principles prediction of the Raman shifts of parahydrogen ($pH_2$) clusters of sizes $N = 4$–19 and 33, based on path integral ground-state simulations with an *ab initio* potential energy surface. The Raman shifts are calculated, using perturbation theory, as the average of the difference-potential energy surface between the potential energy surfaces for vibrationally excited and ground-state parahydrogen monomers. The radial distribution of the clusters is used as a weight function in this average. Very good overall agreement with experiment [G. Tejeda, J. M. Fernández, S. Montero, D. Blume, and J. P. Toennies, Phys. Rev. Lett. **92**, 223401 (2004)] is achieved for $p(H_2)_{2-8,13,33}$. A number of different pair potentials are employed for the calculation of the radial distribution functions. We find that the Raman shifts are sensitive to slight variations in the radial distribution functions. © *2014 AIP Publishing LLC*. [http://dx.doi.org/10.1063/1.4885275]

## I. INTRODUCTION

The study of $pH_2$ clusters is of considerable interest because of their potential superfluid properties. $pH_2$ is a molecular boson with low mass and weak intermolecular forces and thus may be expected to display superfluid properties under appropriate conditions, particularly when in the form of nano-clusters that retain liquid-like properties below the $pH_2$ triple point.[1] The results of early experiments implied the presence of superfluidity in such clusters embedded in helium nanodroplets based on rovibrational Q branch behavior of dopants.[2–5] The first direct measurement of the superfluid fraction was only recently conducted through comparisons of the results of Path Integral Monte Carlo (PIMC) simulations with experimental data involving $pH_2$ clusters of varying sizes, probed using infrared spectroscopy of a $CO_2$ chromophore.[6] Recent advances in PIMC techniques have allowed the accurate simulation of more complex asymmetric top dopants[40] and have been applied to the case of $pH_2$ clusters doped with $H_2O$[7] and $SO_2$[8] molecules. Highly accurate Potential Energy Surfaces (PESs) that describe the molecular interactions are required for simulations of this type. The quality of a PES can be tested by using it to predict the vibrational band origin shift of a chromophore when perturbed by surrounding "solvent" cluster molecules. Li *et al.* demonstrated, for instance, that it is possible to obtain accurate shifts from theory and simulation for the case of $CO_2$ in He and $pH_2$ clusters of various sizes.[6,9]

An interesting question remains regarding what will occur if the chromophore is another $pH_2$, i.e., if we have a pure $pH_2$ cluster. Several PIMC studies have been carried out for pure $pH_2$ clusters at finite temperature[10–14] and in the ground state using the Path Integral Ground-State (PIGS) formulation,[15–17] and Diffusion Monte Carlo (DMC)[18] to elucidate their structural, energetic, and superfluid nature. A summary of these studies has been presented in a review by Navarro and Guardiola.[19] However, some of these studies have shown that the choice of interaction potential used in a simulation affects the details of predicted properties.[15,16,20,21] This reinforces the need to test PESs via comparison of calculated band-origin shifts with experiment. Figure 1 depicts the nature of the band origin shift for the fundamental vibrational energy transition of a $pH_2$ chromophore in a $pH_2$ cluster. Care must be taken in modelling these systems because the $pH_2$ chromophore is indistinguishable from the solvent $pH_2$, and bosonic exchange interactions will result in the delocalization of vibrational excitations.

Two recent developments stimulated this line of inquiry. Tejeda *et al.* overcame difficulties in studying liquid pure $pH_2$ clusters by using cryogenic free-jet expansions to produce clusters of varying sizes resolved in space and time, thereby allowing their clear observation with Raman spectroscopy.[22] They also developed an empirical 1D Lennard-Jones model to fit their data that represents the difference between the PESs for the ground and the first vibrationally excited state of the chromophore. That model predicts vibrational band-origin shifts quite well when perturbatively combined with DMC calculated radial distribution functions of the $pH_2$ clusters. In independent work,[23] Hinde constructed a six-dimensional *ab initio* PES for the pair interaction between $H_2$ and used it to calculate infrared and Raman transition energies within $(H_2)_2$, showing good agreement with the experiments.[22]

In the present paper, the 6D Hinde PES[23] is used to obtain a reduced-dimension set of 1D $pH_2$ dimer PESs by solving a rovibrational Hamiltonian of the $pH_2$ monomers.[24] The difference between the PES in which one quantum of vibrational excitation is distributed amongst the monomers, and the one in which both $pH_2$ monomers are in their vibrational ground states is obtained. This difference-PES is then used to predict vibrational band origin shifts in many-body $pH_2$ clusters from first-principles, by averaging this difference-potential weighted by the radial distribution functions for various

a)Electronic mail: pnroy@uwaterloo.ca

 

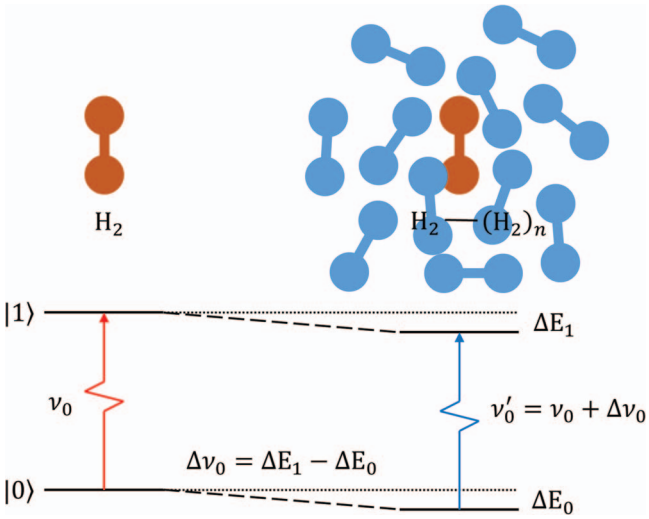


FIG. 1. Schematic of the band origin shift of a "*para*-$H_2$" chromophore in a *para*-$H_2$ cluster.

cluster sizes. The results are tested against the experimental observations of Tejeda *et al.*[22] and predictions generated from their empirical difference-PES. The remainder of this paper is organized as follows: Theoretical and methodological details are introduced in Sec. II, results are presented and discussed in Sec. III, and we close with concluding remarks in Sec. IV.

## II. THEORY AND METHODS

Vibrational band-origin shifts are defined as the difference between the vibrational transition energy of the free chromophore molecule and that of the chromophore molecule in the cluster. This can also be described as the difference between the changes in the upper, $v_t = 1$, and lower, $v_t = 0$, vibrational energies when the free chromophore is introduced into the cluster. For the fundamental vibrational transition of a chromophore in a cluster size of $N$, this may be written as

$$\Delta\nu_0^{[N]} = \Delta E_{\text{cluster}}^{[N]} - \Delta E_{\text{free}} = E_{v_{t=1}}^{[N]} - E_{v_{t=0}}^{[N]}, \qquad (1)$$

in which $\Delta E_{\text{free}}$ is the vibrational spacing of a free molecule, $\Delta E_{\text{cluster}}^{[N]}$ is that spacing when the molecule is in a cluster of $N$ $p\text{H}_2$ molecules, and $E_{v_t}^{[N]}$ is the energy of the system expressed relative to the dissociation limit for $N$ $p\text{H}_2$ molecules when the *total* number of vibrational quanta of the $p\text{H}_2$ monomers is either $v_t = 1$ or 0.

Direct calculation of these energies or energy shifts via simulation poses a challenge. Conventionally, two simulations per cluster size would be undertaken, one with the chromophore in the ground vibrational state and the other with the chromophore in first vibrationally excited state. The total energies of the simulated clusters will eventually converge to the statistical ensemble average values and their difference relative to the free chromophore in either state will give the vibrational band origin shift. However, a PIMC study of $CO_2$ in He clusters found very slow convergence of the statistical errors when increasing the number of simulation steps.[9] Furthermore, in this case of pure $p\text{H}_2$ clusters, an individual molecule should not be singled out and specified as the chromophore in different excitation states during simulation, due to the presence of exchange interactions. Fortunately, a perturbative approach exists to predict the shifts that converges faster by making direct use of the difference between the PESs of the ground and first vibrationally excited states of the chromophore while performing a simulation of just the ground vibrational state of the clusters.[9,22]

We begin by noting that the Hamiltonian for the $v_t = 1$, the vibrational state of the cluster is nearly identical to that in the $v_t = 0$ state, except for the small difference in their potential energies. Here "t" indicates the total quanta of vibrational excitation among the cluster molecules, considering that the excitation can be diffuse due to exchange. Note that if clusters have a more rigid structure,[16] they could potentially be trapped in a metastable state that would prevent the vibrational excitation to be delocalized across the whole cluster. We have not investigated this effect here and therefore assume that the state of the cluster is totally symmetric upon identical particle permutations. The excited state Hamiltonian can therefore be defined approximately as

$$\hat{H}_{v_t=1} \approx \hat{H}_{v_t=0} + \Delta\hat{V}^{[N]}, \qquad (2)$$

in which $\Delta\hat{V}^{[N]} \equiv \hat{V}_{v_t=1}^{[N]} - \hat{V}_{v_t=0}^{[N]}$ is the difference between the total potential energy functions of clusters of size $N$ when one chromophore is in its ground or its first excited state, in which $N$ includes the chromophore in the count. First-order perturbation theory then gives the vibrational frequency shift as

$$\Delta\nu_0^{[N]} = \left\langle \Psi_0^{[N]} \middle| \Delta\hat{V}^{[N]} \middle| \Psi_0^{[N]} \right\rangle, \qquad (3)$$

in which $|\Psi_0(R)|^2$ is the probability in one dimension of finding a solvent $p\text{H}_2$ molecule at a radial distance $R$ from the chromophore, given by the radial distribution function of the cluster, and $\Delta\hat{V}^{[N]}$ is given by the addition of pairwise evaluations of the difference-potential for each $p\text{H}_2$ at each position. With this knowledge, Eq. (3) becomes

$$\Delta\nu_0^{[N]} = (N-1)\int_0^\infty \Delta V^{1\text{D}}(R)\,\rho^{[N]}(R)\,dR, \qquad (4)$$

in which the scaling prefactor of $(N-1)$ accounts for the normalization of the radial distribution function $\rho^{[N]}(R)$, and $\Delta V^{1\text{D}}$ is the difference-PES reduced to one dimension. Note that the Jacobian factor of $R^2$ is absorbed in our definition of the radial distribution function.

Tejeda *et al.* obtained an empirical Lennard-Jones 1D difference-PES for pure $p\text{H}_2$ clusters of the form $\Delta V_{\text{emp}}^{1\text{D}}(R) = \alpha R^{-12} + \beta R^{-6}$, with the parameters $\alpha$ and $\beta$ being determined by fitting their simulated shifts to their Raman spectroscopic data for the frequency shifts, using a weight distribution function $\rho^{[N]}(R)$ obtained from DMC calculations.[22] Generation of higher dimensional distribution functions is computationally prohibitive, necessitating the formulation of reduced 1D PESs to accompany the radial distribution functions.

Hinde's 6D PES must, therefore, first be reduced to effective 1-D potentials for the $v_t = 0$ and $v_t = 1$ vibrational states. For our *ab initio* study, Fig. 2 shows the degrees of freedom expressed in Jacobi coordinates for an interacting pair of $p\text{H}_2$. Those are the coordinates used to represent the 6D PES, $V^{6\text{D}}(R, r_1, r_2, \theta_1, \theta_2, \phi)$. In order to obtain a 1D PES, we use

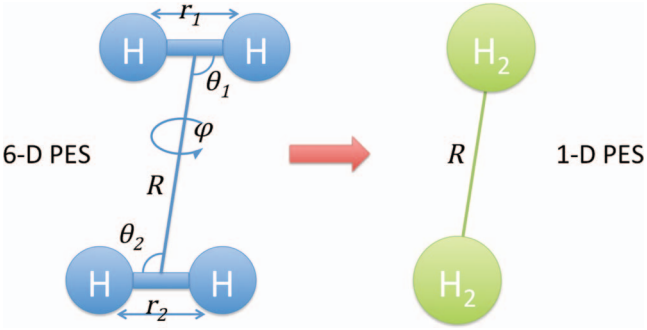


FIG. 2. Schematic of PES reduction.[24]

the Adiabatic Hindered Rotor (AHR) approach established by Li *et al.*, who employed it for calculating vibrational frequency shifts for $CO_2$ in $pH_2$ clusters.[6,24,25] It was shown that the AHR approach preserves some rotational details of the interacting system that a simple spherical average does not.[24,26] In the AHR approach a five-dimensional intermolecular rovibrational Hamiltonian is diagonalized for a set of fixed $R$ values and the locus of lowest eigenvalues define the reduced 1D PES. In the space fixed frame, the Hamiltonian for the $(H_2)_2$ dimer is

$$\hat{H}^{\mathrm{AHR}}(R) = \hat{h}_1^{\mathrm{rovib}}(\mathbf{r_1}) + \hat{h}_2^{\mathrm{rovib}}(\mathbf{r_2}) + V^{6\mathrm{D}}(R, r_1, r_2, \theta_1, \theta_2, \phi), \tag{5}$$

where $\hat{h}_i^{\mathrm{rovib}}$ is the kinetic rovibrational Hamiltonian operator of the $i$th $H_2$ monomer molecule. However, we directly incorporate $pH_2$ monomer rovibrational kinetic energies that were precomputed by Ref. 27 instead of specifying our own $\hat{h}_i^{\mathrm{rovib}}$.

The $pH_2$ monomer rovibrational radial wavefunctions of Ref. 27 ($\psi_{v_i}^{j_i}(r_i)Y_{j_i m_i}(\theta_i, \phi_i) = \langle r_i|v_i j_i\rangle\langle\theta_i|j_i m_i\rangle\frac{e^{im_i\phi_i}}{\sqrt{2\pi}}$) are used as primitive basis functions for constructing the Hamiltonian matrix. For the $pH_2$ molecule, only even rotational states ($j = 0, 2, 4$) are allowed due to the singlet nature of the nuclear spin wavefunction. Moreover, the total wavefunction of the dimer must be symmetric upon the exchange of the two $pH_2$ bosonic monomers. These symmetry requirements will impose restrictions on the nature of the allowed physical basis states. Furthermore, we represent our basis in terms of $\phi = \phi_1 - \phi_2$, since the potential only depends on the relative $\phi$. Additionally, we wish to base our 1D AHR potential on the ground state of the Hamiltonian, such that we choose $m_1 + m_2 = 0$. Finally, for simplicity we convert to real spherical harmonic functions. The basis functions for the dimer will thus have the following form (with $m \equiv m_1$),

$$\begin{aligned}&\langle r_1 r_2 \theta_1 \theta_2 \phi|v_t j_1 j_2 m\rangle \\ &= \frac{1}{\alpha}[\langle r_1|v_1 j_1\rangle\langle\theta_1|j_1 m\rangle\langle r_2|v_2 j_2\rangle\langle\theta_2|j_2 - m\rangle \\ &\quad + \langle r_1|v_2 j_2\rangle\langle\theta_1|j_2 - m\rangle\langle r_2|v_1 j_1\rangle\langle\theta_2|j_1 m\rangle]\cos(m\phi), m \geq 0,\end{aligned} \tag{6}$$

where the normalization factor $\alpha$ is determined explicitly for each matrix element since it varies due to the presence or lack of cross terms when expanding basis functions for certain matrix elements. The Hamiltonian spans only $m \geq 0$ because the symmetry of the basis functions causes cancellation of $m < 0$ matrix elements. The full derivation of the basis functions is available in the supplementary material.[28] For the $v_t = 1$ case, we arbitrarily set $v_1 = 1$ and $v_2 = 0$ and the basis function symmetry accounts for the exchange of the vibrational excitation between the two $pH_2$ monomers. The difference-potential $\Delta V^{1\mathrm{D}}(R)$ is then simply the difference between the two 1D PESs obtained after direct diagonalization of the Hamiltonian matrix for the $v_t = 0$ and $v_t = 1$ cases.

The radial distribution functions of the clusters used in the perturbative model were generated from Langevin equation Path Integral Ground State (LePIGS) simulations, which is a molecular dynamics transmutation of the PIMC PIGS method and offers more simple formulation, since specialized Monte Carlo moves are not required.[29,30] In turn, the PIMC implementation of PIGS is an improvement over DMC methods because it does not suffer from the population-size bias issue affecting convergence in the latter.[31] Thus, LePIGS has two-fold advantages over the DMC method. Multiple radial distributions for each cluster size were generated for comparison via LePIGS using a number of different $pH_2$ interaction potentials that were described in earlier studies.[23,32–34] The Hinde[23] and Szalewicz[34] potentials are *ab initio* potential functions, while the Silvera-Goldman[33] and Buck[32] potentials are empirical functions that were parameterized to conform to different types of experiments. For cluster sizes of $N = 4$ and above, a Jastrow-type trial wavefunction[15] is used in the simulations. Unfortunately, smaller clusters were too weakly bound and dissociated during simulation when this trial wave function was used. Instead, a direct calculation is used for $N = 2$ and a perturbative approach is used for $N = 3$. The simulation parameters were optimized using the $N = 4$ cluster, resulting in a thermodynamic $\beta$ value of 1.00 $\mathrm{K}^{-1}$, $\tau$ of 0.003 $\mathrm{K}^{-1}$, time step of 5 fs, and 0.2 ps skipped between trajectory output to obtain decorrelated data. The simulations were run for 20 ns.

The output of the simulation trajectories contains a series of positions where the $pH_2$ are located at each step. These are converted to raw radial distributions by calculating all $pH_2$-$pH_2$ pair distances. These raw radial distributions are directly used to calculate vibrational shifts instead of further processing them into radial distribution *functions*, $g(r)$, in order to maintain accuracy (however, the various associated $g(r)$ plots are available in the supplementary material[28]). The value of the difference-PES is then sampled for each of those raw pair distances and the results averaged. This turns Eq. (4) into

$$\Delta v_0^{[N]} = \frac{1}{n}\sum_i^n \Delta V^{1\mathrm{D}}\left(R_i^{[N]}\right), \tag{7}$$

in which $n$ is the number of data points in the simulation trajectory for a particular cluster.

## III. RESULTS AND DISCUSSION

Vibrational frequency shifts calculated for clusters using various radial distributions and two choices of the difference-potential are presented in Fig. 3. Results in the upper panel were obtained using the *ab initio* 1D difference-potential derived from Hinde's 6D PES[23] while those in the lower panel were generated using the empirical difference-potential of

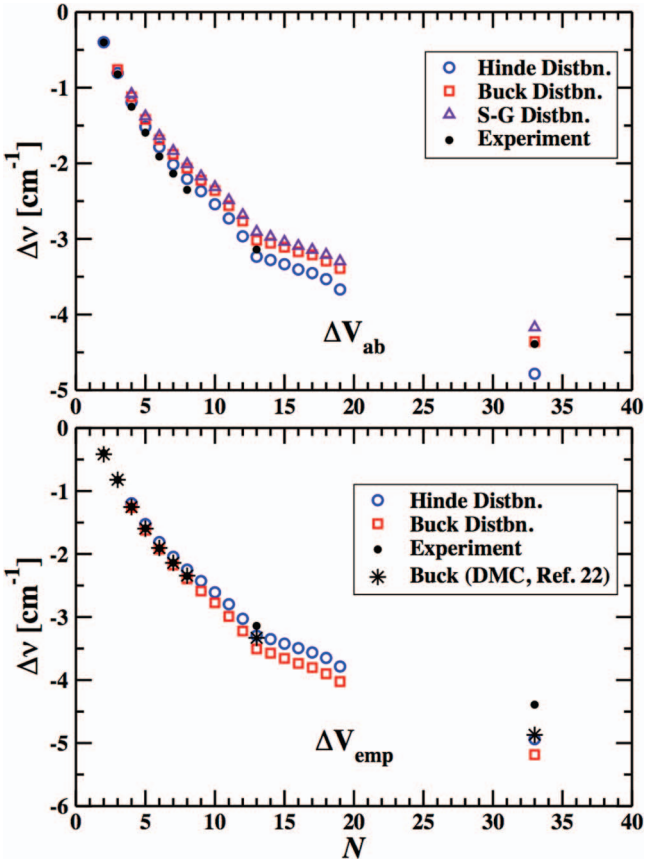


FIG. 3. Variation with cluster size of predicted vibrational frequency shifts calculated using radial distributions generated from different simulation potentials (see key). Upper Panel: Results obtained using *ab initio* difference-potential. Lower Panel: Results obtained using empirical difference-potential.

Ref. 22. In the upper panel, the shifts predicted with radial distributions obtained from the *ab initio* Hinde potential simulations (blue open circles) are in better agreement with experiment (filled circles) at small cluster sizes ($N < 13$), where shifts predicted with radial distributions using the Buck potential (red open squares) simulations are systemically less negative than those from the Hinde results and from experiment. The agreement is reversed at large cluster sizes ($N > 13$), where shifts obtained from the Hinde radial distributions become more negative compared to the experiment, while the Buck distribution prediction at $N = 33$ agrees with the experimental result. A feature of note present in all series of shifts is the change in slope of the trend in shifts with respect to the cluster size at $N = 13$, a magic number.

The shifts obtained using distributions generated from four different potentials, together with the experimental values, are tabulated in Table I. The discrepancy between the predicted vibrational frequency shifts at small and large cluster sizes from the different radial distributions might be explained by the origin of the potentials. The Hinde potential is an accurate *ab initio* pair potential that should perform better for small clusters where pair interactions dominate. A similar trend in the predicted shifts (not shown in Fig. 3) was observed for distributions generated using the *ab initio* Szalewicz potential, in that they are closer to experiment at small cluster sizes but are more negative for $N = 13$ and 33. Perhaps at larger cluster sizes many-body effects become prominent, which these *ab initio* pure pair potentials do not account for. This hypothesis may be supported by the fact that predictions generated using the Silvera-Goldman distributions that perform better than the *ab initio* potential distributions at $N = 33$, shown in the upper panel of Fig. 3, considering that

TABLE I. $\Delta\nu_0$ (cm$^{-1}$) obtained from radial distributions generated using different potentials and the two $\Delta$V. Standard errors are $\leq$0.005 cm$^{-1}$. Experimental (Expt.) are provided for comparison purposes.

| | $\Delta\nu_0$, $\Delta V_{ab}$ | | | | | $\Delta\nu_0$, $\Delta V_{emp}$ | | | | |
|---|---|---|---|---|---|---|---|---|---|---|
| *N* | Expt.[22] | Hinde | Szalewicz | Buck | S-G | Buck DMC[22] | Hinde | Szalewicz | Buck | S-G |
| 4 | −1.251 | −1.19 | −1.203 | −1.118 | −1.092 | −1.255 | −1.197 | −1.223 | −1.261 | −1.180 |
| 5 | −1.594 | −1.517 | −1.527 | −1.417 | −1.385 | −1.597 | −1.527 | −1.566 | −1.622 | −1.515 |
| 6 | −1.910 | −1.785 | −1.800 | −1.683 | −1.648 | −1.904 | −1.812 | −1.863 | −1.923 | −1.809 |
| 7 | −2.136 | −2.016 | −2.025 | −1.878 | −1.852 | −2.141 | −2.045 | −2.098 | −2.175 | −2.043 |
| 8 | −2.350 | −2.206 | −2.217 | −2.059 | −2.028 | −2.344 | −2.248 | −2.315 | −2.392 | −2.257 |
| 9 | | −2.369 | −2.384 | −2.219 | −2.181 | | −2.431 | −2.493 | −2.588 | −2.447 |
| 10 | | −2.542 | −2.553 | −2.367 | −2.335 | | −2.611 | −2.674 | −2.774 | −2.628 |
| 11 | | −2.729 | −2.750 | −2.545 | −2.516 | | −2.800 | −2.887 | −2.990 | −2.821 |
| 12 | | −2.965 | −2.981 | −2.752 | −2.702 | | −3.028 | −3.109 | −3.222 | −3.036 |
| 13 | −3.140 | −3.236 | −3.276 | −3.010 | −2.922 | −3.330 | −3.297 | −3.405 | −3.507 | −3.270 |
| 14 | | −3.279 | −3.289 | −3.043 | −3.002 | | −3.352 | −3.449 | −3.573 | −3.369 |
| 15 | | −3.334 | −3.339 | −3.111 | −3.064 | | −3.425 | −3.519 | −3.657 | −3.452 |
| 16 | | −3.404 | −3.404 | −3.160 | −3.122 | | −3.495 | −3.595 | −3.736 | −3.529 |
| 17 | | −3.453 | −3.472 | −3.209 | −3.175 | | −3.566 | −3.665 | −3.802 | −3.606 |
| 18 | | −3.532 | −3.550 | −3.284 | −3.250 | | −3.651 | −3.753 | −3.899 | −3.694 |
| 19 | | −3.668 | −3.683 | −3.378 | −3.333 | | −3.787 | −3.892 | −4.024 | −3.793 |
| 33 | −4.390 | −4.784 | −4.811 | −4.423 | −4.169 | −4.870 | −4.941 | −5.085 | −5.183 | −4.794 |

the version of the Silvera-Goldman potential used includes an effective many-body term that was fit to solid state data.[33] However, the Buck potential distributions also appears to perform well at large cluster sizes even though it has been obtained from a fit to scattering cross section data, and scattering is an inherently two-body process, meaning the Buck potential is a pure pair potential.[32] This suggests that the good performance of the empirical potential distributions at large cluster sizes may simply be an accident. In fact, the Raman spectral peaks for the $N = 13$ and 33 clusters were unresolved as reported in Ref. 22 and we can deduce a large error in the experimentally observed shifts from the broad peak widths, which might account for some of our discrepancy.

The change in slope of all the sets of predicted shifts at $N = 13$ occurs because the first solvation shell of the cluster is completed at that point. The first solvation shell makes a larger contribution to the shift compared to outer shells because the peak of its distribution is situated closer to the minimum of the difference-potential, so there is a steeper slope in the trend of shifts as it gets filled. The lower panel in Fig. 3 presents shifts predicted using the empirical Lennard-Jones difference-potential reported by Tejeda *et al.* It also shows the predicted shifts that they calculated using DMC radial distributions generated from the Buck potential. Shifts using the empirical difference-potential are good for the small cluster sizes, as is to be expected, since a fit to observed shifts was used to define the empirical difference-potential. However, they all diverge from experiment in the same manner at large cluster sizes. This may be expected because the empirical difference-potential was defined by a fit to the experimental shifts for only $N = 2$–8 clusters that had resolved Raman spectral peaks. Interestingly, our LePIGS radial distributions using the Buck potential do not fully reproduce those shifts predicted by the earlier DMC distributions, despite using the same potential. This may be attributed to LePIGS distributions being less noisy than those of Ref. 22.

A comparison of the empirical 1D difference-potential from Ref. 22 with the one we determine from the 6D *ab*

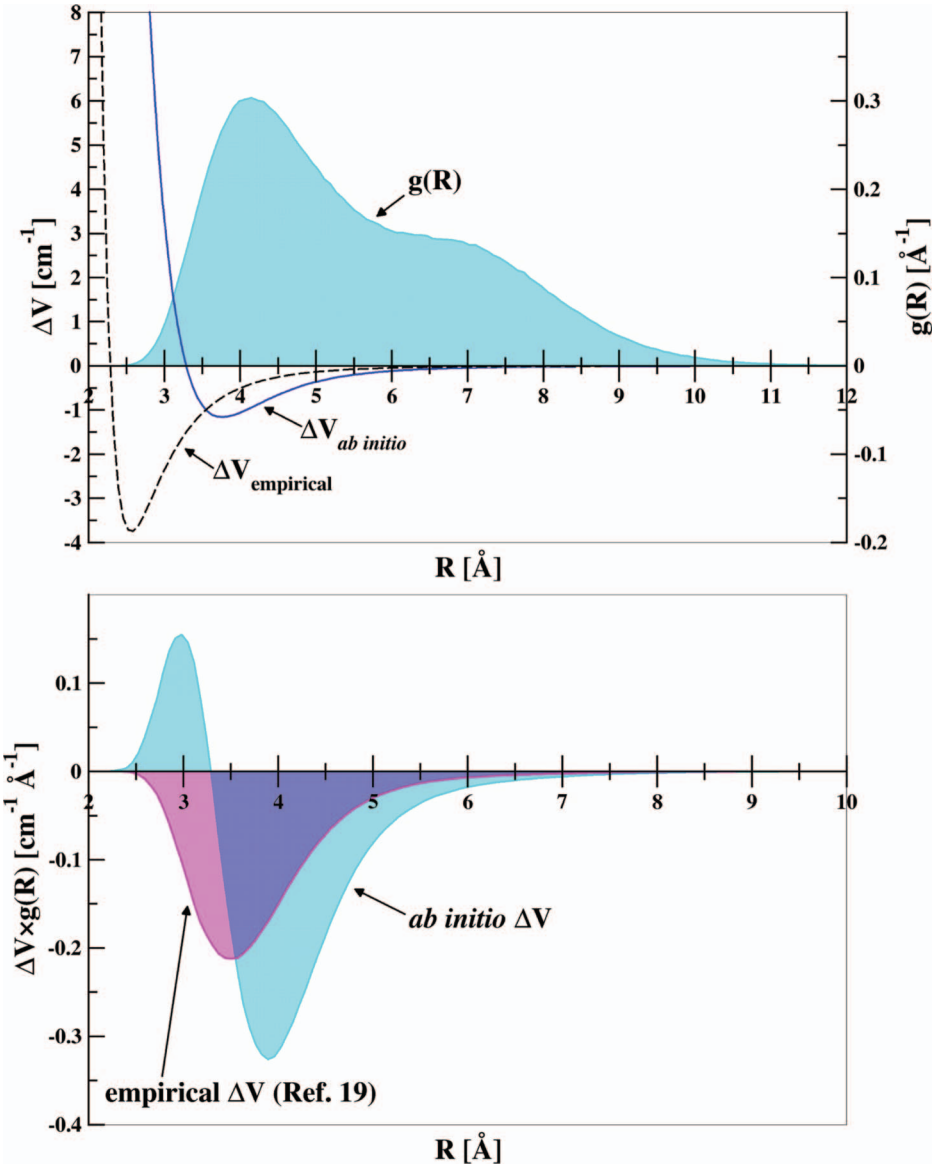


FIG. 4. Upper Panel: Comparison of difference-potentials beside an $N = 8$ radial distribution function. Lower Panel: The integrand of Eq. (4) for the two difference-potentials when combined with the $N = 8$ radial distribution function.

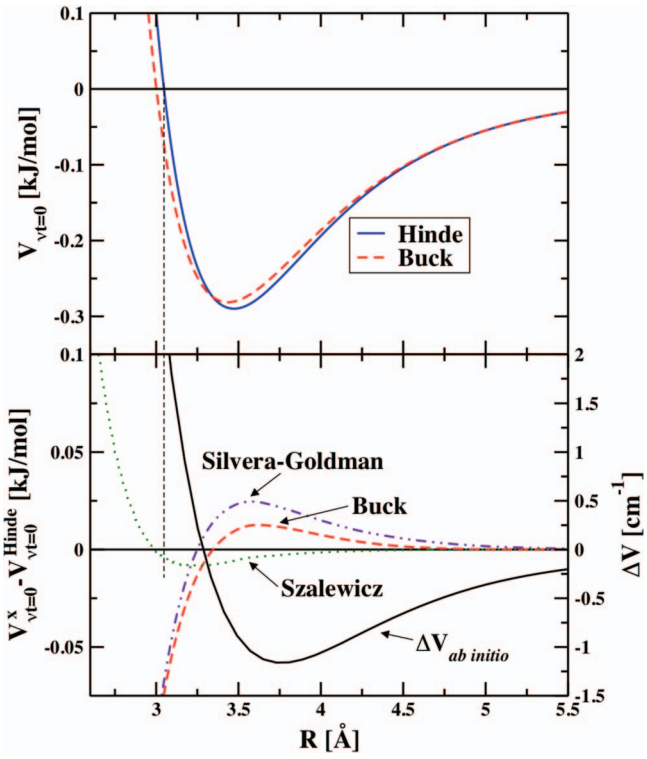


FIG. 5. Upper Panel: Key ground vibrational state 1-D potentials used in simulation to generate radial distributions. Lower Panel: Differences of various 1-D potentials with the *ab initio* potential of Hinde.

*initio* Hinde PES is shown in the upper panel of Fig. 4. There is a marked difference in the position and depth of the potentials, despite similar shift predictions for small $N$, with the empirical difference-potential having a much deeper well that is centered at a much shorter distance. Thus, the difference-potentials probe the radial distributions with different emphases, e.g., the region where the empirical difference-potential is most strongly negative is only sampled by the inner tail of the radial distribution functions as shown in the upper panel of Fig. 4 for an $N = 8$ cluster, while the region where the empirical difference-potential turns positive is not sampled at all. In contrast, the radial distribution functions sample both positive and negative domains of the *ab initio* difference-potential. Additional insight into the reasons why the empirical and *ab initio* difference-potentials give similar predictions of shifts for small clusters is given by the lower panel of Fig. 4. It depicts plots of the integrand of Eq. (4) for the two difference-potentials and the $N = 8$ distribution. The shapes of the empirical and *ab initio* integrand curves are different due to the wells and repulsive walls of the difference-potentials matching up with different portions of the radial distribution function, however the net area under the curves representing the shifts is similar. The *ab initio* difference-potential is clearly the correct one and this result illustrates the difficulty of determining empirical difference-potentials using bulk-averaging.

A comparison of the four 1D potentials used to generate the radial distributions is presented in Fig. 5. The top panel compares a plot of the 1D $v_t = 0$ potential we generated from the 6D *ab initio* Hinde PES with the empirical Buck potential. The bottom panel shows plots of the difference between

TABLE II. Direct calculation of shift for $pH_2$ dimer.

| Method | $\Delta\nu_0$ ($cm^{-1}$) |
|---|---|
| Observed | −0.400 |
| Tejeda *et al.*: $\Delta V_{emp}(R)$[22] | −0.417 |
| Hinde: direct *ab initio*[23] | −0.405 |
| Our Work: $\Delta V_{ab}(R)$ | −0.399 |

the Hinde potential and other 1D potentials used to generate radial distribution functions, together with a plot of the Hinde difference-potential $\Delta V_{ab}$ (black solid line). In the well region of the potentials, the Buck (red dashed line) and Silvera-Goldman (purple dashed-dotted line) potentials are less attractive than the Hinde potential. This means the $pH_2$ are less bound to the vicinity of the potential minima, and their radial distributions can seep further inward or outward. This will result in a less negative shift for the Buck and Silvera-Goldman potentials relative to the Hinde potential because there is less probing of the attractive well of the difference-potential. In addition, in the region of the repulsive walls the Buck and Silvera-Goldman potentials are less repulsive than the Hinde potential, indicating they have gentler slopes. This means the $pH_2$ particles can approach closer together in those cases and this will give rise to larger values for the radial distributions at short distances. In this region the difference-potential is positive and so will again tend to produce less negative shifts when combined with the larger radial distributions of the Buck and Silvera-Goldman cases relative to the Hinde potential case. The Szalewicz potential (green dotted line) is slightly deeper than the Hinde potential in the region of the potential well, meaning the radial distributions are more concentrated at the potential minimum, and more positive in the later part of the repulsive wall region, indicating a steeper slope. This leads to slightly more negative shifts relative to the Hinde potential case.

Simulations to obtain a dimer or trimer radial distribution with LePIGs is not possible because the clusters rapidly dissociate. Instead, for the $N = 2$ dimer the eigenvalue problem in $R$ was solved using exact diagonalization with a Colbert-Miller Discrete Variable Representation (DVR) basis[35] after reduction of the Hinde PES for the ground and first vibrational states, with the resulting energy difference between them giving the vibrational frequency shift for the dimer. As shown in Table II, the result is in good agreement experiment and with the binding energy calculations Hinde carried out himself.

To obtain the shift for the $N = 3$ trimer, we employed the usual perturbative approach using the *ab initio* difference-potential, with the trimer ground state radial pair density being obtained from exact diagonalization using the approach of Refs. 36–38 and 15. The ground state interaction potential used in the evaluation was either the ground vibrational state Hinde potential or the Buck potential. The result shown in Table III shows good agreement with experiment for the Hinde potential case.

For comparison purposes, we have also calculated the vibrational shift based on the spherical averaging of the 6D Hinde hydrogen potential for the difference potential. Results are presented in the supplementary material.[28] The AHR

TABLE III. Perturbative calculation of shift for $pH_2$ trimer.

| Method | $\Delta\nu_0$ ($cm^{-1}$) |
|---|---|
| Observed | −0.822 |
| Tejeda *et al.*: $\Delta V_{emp}(R)$[22] | −0.821 |
| $\Delta V_{ab}(R)$, empirical Buck $V_{v_t=0}$ | −0.748 |
| $\Delta V_{ab}(R)$, *ab initio* Hinde $V_{v_t=0}$ | −0.807 |

results generally agree better with experiments for clusters with $3 \leq N \leq 8$. For the dimer ($N = 2$) the AHR and spherically averaged results are essentially the same within error bars. The spherically averaged difference potential however leads to a better agreement with experiment for $N = 13, 33$. Future work will focus on a detailed analysis of these differences.

## IV. CONCLUSIONS

In conclusion, we have described the development and application of *ab initio* reduced PESs for the prediction of Raman spectral shifts of pure para-hydrogen clusters. The results confirm that the 6D Hinde PES is a high quality pair PES, with its reduced 1D surfaces predicting shifts in good agreement with experiment for small cluster sizes including the $(pH_2)_2$ dimer. However, for a cluster size of $N = 33$, the shift predicted using radial distributions generated from the ground state reduced Hinde potential was more negative than the experimental one. In that domain, radial distributions generated from empirical potentials performed better, through accident in the case of the Buck potential or possibly by accounting for many-body effects that may become non-negligible after the first solvation shell in the case of the Silvera-Goldman potential. By combining radial distributions generated from these empirical potentials and the *ab initio* difference-potential, we are able to extend the prediction of shifts to large $pH_2$ cluster sizes that have not yet been observed, such as those we have shown between N = 13 and 33. If this were done with the empirical Lennard-Jones difference-potential, those predicted shifts would diverge from experiment, as is expected at the large cluster sizes that it was not parameterized for. However, it is clear that our *ab initio* difference-potential is closer to physical reality. Future work will involve the assessment of the importance of many-body effects that may account for the difference between our predictions and the result of experiment for $N = 33$. In that regard, the work of Hinde[39] on three-body effects on the energy of the $H_2$ trimer will be of interest. One other possibility worth exploring is an incorrect assignment of the experimental vibrational shift for $N = 33$ as suggested in Ref. 20.

## ACKNOWLEDGMENTS

We thank Professor R. J. Hinde for providing us with the latest version of his 6D $(H_2)_2$ PES code. We also thank Professor S. Hopkins and Professor M. Nooijen for fruitful discussions. P.-N.R. acknowledges financial support from the Natural Sciences and Engineering Research Council of Canada (NSERC), the Ministry of Research and Innovation (MRI) of Ontario, and the Canada Foundation for Innovation (CFI). R.J.L.R. thanks NSERC for support. Matthew Schmidt acknowledges NSERC for a graduate scholarship.

[1] T. Zeng and P.-N. Roy, Rep. Prog. Phys. **77**, 046601 (2014).
[2] S. Grebenev, B. Sartakov, J. P. Toennies, and A. F. Vilesov, Science **289**, 1532 (2000).
[3] S. Grebenev, B. Sartakov, J. P. Toennies, and A. Vilesov, Phys. Rev. Lett. **89**, 225301 (2002).
[4] S. Grebenev, B. G. Sartakov, J. P. Toennies, and A. F. Vilesov, Europhys. Lett. **83**, 66008 (2008).
[5] S. Grebenev, B. G. Sartakov, J. P. Toennies, and A. F. Vilesov, J. Chem. Phys. **132**, 064501 (2010).
[6] H. Li, R. J. Le Roy, P.-N. Roy, and A. R. W. McKellar, Phys. Rev. Lett. **105**, 133401 (2010).
[7] T. Zeng, H. Li, and P.-N. Roy, J. Phys. Chem. Lett. **4**, 18 (2013).
[8] T. Zeng, G. Guillon, J. T. Cantin, and P.-N. Roy, J. Phys. Chem. Lett. **4**, 2391 (2013).
[9] H. Li, N. Blinov, P.-N. Roy, and R. J. Le Roy, J. Chem. Phys. **130**, 144305 (2009).
[10] P. Sindzingre, D. M. Ceperley, and M. L. Klein, Phys. Rev. Lett. **67**, 1871 (1991).
[11] M. C. Gordillo and D. M. Ceperley, Phys. Rev. B **65**, 174527 (2002).
[12] F. Mezzacapo and M. Boninsegni, Phys. Rev. Lett. **97**, 045301 (2006).
[13] F. Mezzacapo and M. Boninsegni, Phys. Rev. A **75**, 033201 (2007).
[14] F. Mezzacapo and M. Boninsegni, Phys. Rev. Lett. **100**, 145301 (2008).
[15] J. E. Cuervo and P.-N. Roy, J. Chem. Phys. **125**, 124314 (2006).
[16] J. E. Cuervo and P.-N. Roy, J. Chem. Phys. **128**, 224509 (2008).
[17] J. E. Cuervo and P.-N. Roy, J. Chem. Phys. **131**, 114302 (2009).
[18] R. Guardiola and J. Navarro, Phys. Rev. A **74**, 025201 (2006).
[19] J. Navarro and R. Guardiola, Int. J. Quantum Chem. **111**, 463 (2011).
[20] S. A. Khairallah, M. B. Sevryuk, D. M. Ceperley, and J. P. Toennies, Phys. Rev. Lett. **98**, 183401 (2007).
[21] F. Mezzacapo and M. Boninsegni, J. Phys.: Conf. Ser. **150**, 032059 (2009).
[22] G. Tejeda, J. M. Fernández, S. Montero, D. Blume, and J. P. Toennies, Phys. Rev. Lett. **92**, 223401 (2004).
[23] R. J. Hinde, J. Chem. Phys. **128**, 154308 (2008).
[24] H. Li, P.-N. Roy, and R. J. Le Roy, J. Chem. Phys. **133**, 104305 (2010).
[25] P. L. Raston, W. Jäger, H. Li, R. J. Le Roy, and P.-N. Roy, Phys. Rev. Lett. **108**, 253402 (2012).
[26] T. Zeng, H. Li, R. J. Le Roy, and P.-N. Roy, J. Chem. Phys. **135**, 094304 (2011).
[27] C. Schwartz and R. J. L. Roy, J. Mol. Spectrosc. **121**, 420 (1987).
[28] See supplementary material at http://dx.doi.org/10.1063/1.4885275 for the various $g(r)$ plots.
[29] S. Constable, M. Schmidt, C. Ing, T. Zeng, and P.-N. Roy, J. Chem. Phys. A **117**, 7461 (2013).
[30] M. Schmidt, S. Constable, C. Ing, and P.-N. Roy, J. Chem. Phys. **140**, 234101 (2014).
[31] M. Boninsegni and S. Moroni, Phys. Rev. E **86**, 056712 (2012).
[32] U. Buck, F. Huisken, A. Kohlhase, D. Otten, and J. Schaefer, J. Chem. Phys. **78**, 4439 (1983).
[33] I. F. Silvera and V. V. Goldman, J. Chem. Phys. **69**, 4209 (1978).
[34] K. Patkowski, W. Cencek, P. Jankowski, K. Szalewicz, J. B. Mehl, G. Garberoglio, and A. H. Harvey, J. Chem. Phys. **129**, 094304 (2008).
[35] D. T. Colbert and W. H. Miller, J. Chem. Phys. **96**, 1982 (1992).
[36] P.-N. Roy, J. Chem. Phys. **119**, 5437 (2003).
[37] Y. D. Liu and P.-N. Roy, J. Chem. Phys. **121**, 6282 (2004).
[38] M. P. Nightingale and P.-N. Roy, J. Phys. Chem. A **110**, 5391 (2006).
[39] R. J. Hinde, Chem. Phys. Lett. **460**, 141 (2008).
[40] E. G. Noya, C. Vega, and C. McBride, J. Chem. Phys. **134**, 054117 (2011).